Evidence of the pair instability gap in the distribution of black hole masses

Hui Tong[1,2*], Maya Fishbach[3,4,5], Eric Thrane[1,2], Matthew Mould[6,7,8], Thomas A. Callister[9], Amanda Farah[10], Nir Guttman[1,2], Sharan Banagiri[1,2], Daniel Beltran-Martinez[11], Ben Farr[12], Shanika Galaudage[13,14], Jaxen Godfrey[12], Jack Heinzel[6,7,8], Marios Kalomenopoulos[15,16], Simona J. Miller[17,18], Aditya Vijaykumar[3]

[1*]School of Physics and Astronomy, Monash University, Clayton, VIC 3800, Australia.

[2*]OzGrav: The ARC Centre of Excellence for Gravitational Wave Discovery, Clayton, VIC 3800, Australia.

[3]Canadian Institute for Theoretical Astrophysics, University of Toronto, 60 St George St, Toronto, ON M5S 3H8, Canada.

[4]David A. Dunlap Department of Astronomy and Astrophysics, University of Toronto, 50 St George St, Toronto, ON M5S 3H8, Canada.

[5]Department of Physics, University of Toronto, 60 St George St, Toronto, ON M5S 3H8, Canada.

[6]LIGO Laboratory, Massachusetts Institute of Technology, Cambridge, MA 02139, USA.

[7]Kavli Institute for Astrophysics and Space Research, Massachusetts Institute of Technology, Cambridge, MA 02139, USA.

[8]Department of Physics, Massachusetts Institute of Technology, Cambridge, MA 02139, USA.

[9]Kavli Institute for Cosmological Physics, The University of Chicago, Chicago, IL 60637, USA.

[10]Department of Physics, , The University of Chicago, Chicago, IL 60637, USA.

[11]Centro de Investigaciones Energéticas Medioambientales y Tecnológicas, Avda. Complutense 40, Madrid, 28040, Spain.

[12]Institute for Fundamental Science, Department of Physics, , University of Oregon, Eugene, OR 97403, USA.

[13] Laboratoire Lagrange, Université Côte d'Azur, Observatoire de la Côte d'Azur, CNRS, Bd de l'Observatoire, 06300, France .
[14] Laboratoire Artemis, Université Côte d'Azur, Observatoire de la Côte d'Azur, CNRS, Bd de l'Observatoire, 06300, France .
[15]Nevada Center for Astrophysics, University of Nevada, Las Vegas, NV 89154, USA.
[16]Department of Physics and Astronomy, University of Nevada, Las Vegas, NV 89154, USA.
[17]Department of Physics, California Institute of Technology, Pasadena, CA 91125, USA.
[18]LIGO Laboratory, California Institute of Technology, Pasadena, CA 91125, USA.

*Corresponding author(s). E-mail(s): hui.tong@monash.edu;

Abstract

Stellar theory predicts a forbidden range of black-hole masses between $\sim$**50**–**130** $M_\odot$ due to pair-instability supernovae, but evidence for such a gap in the mass distribution from gravitational-wave astronomy has proved elusive. Early hints of a cutoff in black-hole masses at $\sim$**45** $M_\odot$ disappeared with the subsequent discovery of more massive binary black holes. Here, we report evidence of the pair-instability gap in LIGO–Virgo–KAGRA's fourth gravitational wave transient catalog (GWTC-4), with a lower boundary of $\mathbf{44}^{+\mathbf{5}}_{-\mathbf{4}} M_\odot$ (90% credibility). While the gap is not present in the distribution of *primary* masses m_1 (the bigger of the two black holes in a binary system), it appears unambiguously in the distribution of *secondary* masses m_2, where $m_2 \leq m_1$. The location of the gap lines up well with a previously identified transition in the binary black-hole spin distribution; binaries with primary components in the gap tend to spin more rapidly than those below the gap. We interpret these findings as evidence for a subpopulation of hierarchical mergers: binaries where the primary component is the product of a previous black-hole merger and thus populates the gap. Our measurement of the location of the pair-instability gap constrains the S-factor for $^{12}\mathbf{C}(\alpha,\gamma)^{16}\mathbf{O}$ at 300keV to $\mathbf{260}^{+\mathbf{190}}_{-\mathbf{108}}$ keV barns.

Stellar theory predicts a lack of black holes with masses from $\sim$50 $M_\odot$ to $\sim$130 $M_\odot$ [1–7]. Stars with initial (zero-age main sequence) masses in the range 100 to 260 $M_\odot$ are expected to experience (pulsational) pair-instability supernovae. At these masses, the carbon–oxygen stellar core is sufficiently hot that photons spontaneously produce electron–positron pairs. This leads to a drop in photon pressure that triggers sudden gravitational collapse, followed by the explosive ignition of oxygen. The resulting stellar explosion is so powerful that it can disrupt the entire stellar core in a pair-instability

supernova, leaving behind no remnant whatsoever. This manifests as a gap in the black hole mass spectrum in the 50–130 $M_\odot$ range. Alternatively, it may trigger a series of pulses that shed enough mass so that the star collapses to a black hole safely below the lower edge of the gap.

Although the existence of pair instability supernovae is a robust prediction of stellar theory, observational evidence has proved elusive. Few examples of (pulsational) pair instability supernova have been observed; promising candidates are the supernova SN2018ibb and SN2020acct [8, 9]. Gravitational-wave observatories provide a new, promising probe of pair-instability supernovae, because they are sensitive to black holes in exactly the relevant mass range [10–12]. Measurements of the mass gap can constrain important theoretical uncertainties, including the role of metallicity, details of neutrino physics, convective mixing efficiency, and nuclear reaction rates [7]. For example, a driving uncertainty in the gap's location is the uncertain $^{12}\mathrm{C}(\alpha,\gamma)^{16}\mathrm{O}$ reaction rate, opening up the possibility to measure this nuclear reaction rate with gravitational-wave observations [7, 13].

However, previous gravitational-wave analyses have not found a clear gap in the distribution of black hole masses [14, 15] (though see Refs. [16–19] which found hints that black holes above $\sim 40\,M_\odot$ do not originate from stellar collapse using GWTC-3). Gravitational waves encode the primary mass m_1 and secondary mass $m_2 < m_1$ of each binary. By combining the binary black-hole events in the gravitational-wave catalog, the joint mass distribution $\pi(m_1, m_2)$ can be inferred. The first gravitational-wave transient catalog (GWTC-1) resulted in preliminary hints for a cutoff in the primary mass distribution at $\sim 45\,M_\odot$ [e.g., 20], but subsequent discoveries of more massive black holes ruled out a sharp m_1 cutoff [21]. Meanwhile, an observed $\sim 35\,M\odot$ peak in the distribution of black-hole primary mass was hypothesized to result from a pileup from pulsational pair-instability supernovae [21, 22], but subsequent work suggests this interpretation is in tension with stellar physics, observed supernovae rates and nuclear physics [23, 24], though see, e.g., Refs. [25] for an alternative view.

While the distribution of primary black-hole masses does not show a clear gap, there have not been studies looking for a gap in the secondary-mass distribution. Black holes that do not form directly from ordinary stellar collapse—such as those that originate from previous black-hole mergers [26], stellar mergers [27, 28], collapsars with significant mass loss from above the gap [29], or which have experienced significant accretion [30, 31]—may contaminate the gap. Such processes are expected to be rare, and therefore unlikely to affect both black holes in a binary. We therefore analyze data from GWTC-4 [32] using a model that specifically searches for a mass gap in the distribution of m_2. We employ a similar mass model formalism as in Ref. [33] to describe the probability distribution $\pi(m_1, m_2)$ by fitting to the model of the primary mass distribution $\pi(m_1)$ and the conditional secondary-mass distribution $\pi(m_2|m_1)$. However, we modify the model to allow for an interval corresponding to the pair-instability gap in m_2, where the probability density is zero [15]; see Equation (3). We assume a default model for black-hole spin from Ref. [33]. The absence of a gap, i.e., the width of the gap to be $< 20\,M_\odot$, is ruled out at 99.9% credibility(see Extended Figure 1). The gap model is preferred over the no-gap model by a natural logarithm

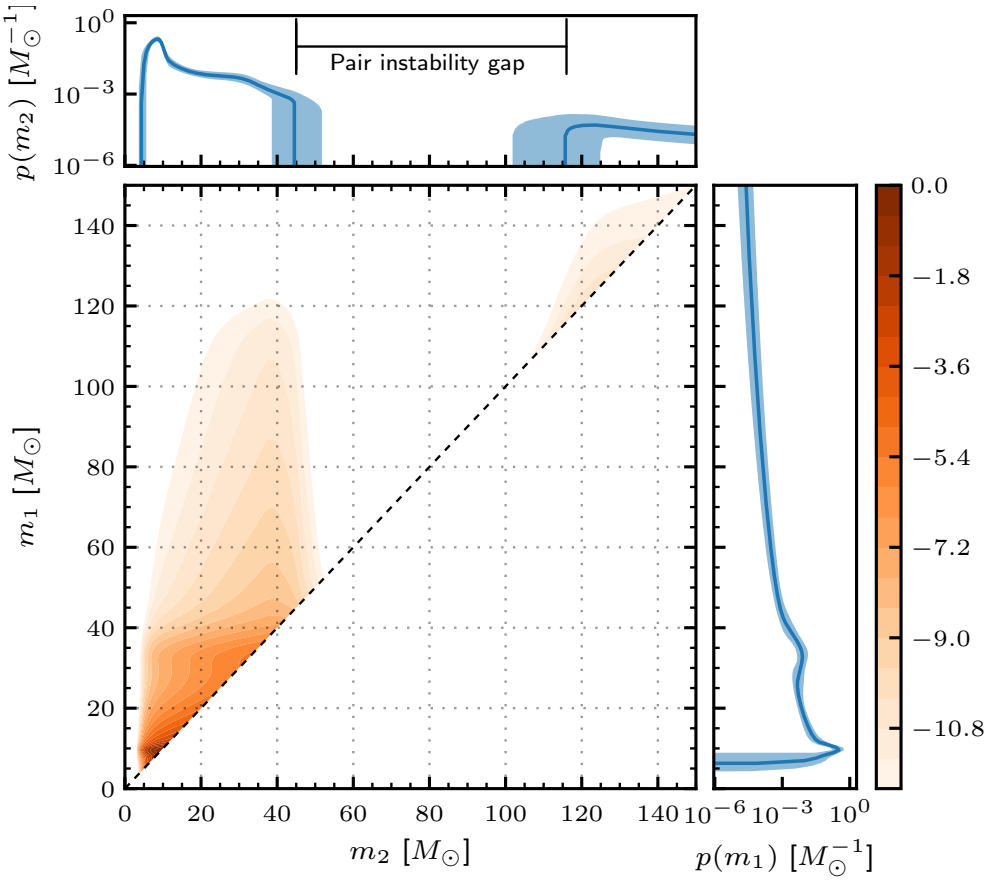

Fig. 1 Reconstructed distribution of binary black-hole masses. The primary mass m_1 is by definition larger than the secondary mass $m_2 < m_1$. The mean prediction of the joint distribution $\pi(m_1, m_2)$ is shown in orange while the median prediction of the marginal distributions $\pi(m_1)$ and $\pi(m_2)$ are shown in solid line in blue with 90% credibility range indicated by the shaded bands. The color bar represents the two-dimensional probability density $\log[p(m_1, m_2)/\max p(m_1, m_2)]$. The "island" of probability at the upper right of the two-dimensional density plane is mostly associated with the high-mass event GW231123.

Bayes factor $\ln \mathcal{B}$ of $\sim$4.4; the priors on the gap parameters as well as the details of the mass and spin models are described in Section 1.2 and Section 1.6.

Figure 1 shows the black hole mass distribution inferred under this model. While the m_1 distribution extends unbroken from $45M_\odot$ to $\sim 120M_\odot$, there is a clear gap in the m_2 distribution with the lower edge at $45^{+7}_{-6}M_\odot$ (90% credibility), remarkably consistent with theoretical predictions for the pair-instability gap [1, 34]. We constrain the upper edge of the gap to be $116^{+9}_{-14}M_\odot$ (90% credibility). However, the upper edge is primarily constrained by GW231123, the most massive binary detected so far [35]. The uncertainty of the upper edge is dominated by the uncertainty in the parameters

of this single event, which may or may not originate from stars massive enough to collapse to the "far side" of the gap, potentially experiencing significant mass loss via disk winds and jet launching [35, 36]. In contrast, the lower edge of the gap is a robust feature of the binary black hole population: excluding GW231123 from the analysis results in a lower edge of $43^{+7}_{-6}\,M_\odot$ and leaves the upper edge unconstrained. Such a gap is also present in the maximum population likelihood distribution [37]—a model-free method to visualise population properties. The maximum population likelihood distribution clearly shows an absence of binary black holes in the m_2 gap region (see Extended Fig. 4 and the detailed discussion in Section. 1.4).

In order to determine if the mass gap was evident prior to GWTC-4, we fit the same model to LIGO–Virgo–KAGRA's third gravitational wave transient catalog (GWTC-3) [38]. With GWTC-3, we infer the lower edge to be $49^{+79}_{-11}\,M_\odot$—consistent with our results from GWTC-4 albeit with significantly greater uncertainty with fewer events.

The clear appearance of the pair instability gap in the distribution of the secondary mass m_2 rather than the primary mass m_1 can be well-understood in the context of hierarchical mergers. Hierarchical mergers include one or more "second-generation" (2G) remnants of previous black-hole mergers. Unlike "first-generation" (1G) black holes that are born from stellar collapse, 2G black holes can populate the pair-instability gap. Hierarchical mergers can occur in dense stellar environments [26]. For hierarchical mergers in dense star clusters with escape speeds typical of globular clusters, most 2G black holes are ejected from the cluster due to the recoil kicks they receive from the anisotropic emission of gravitational waves [39, 40]. Only a small fraction are retained so that they might merge again with another black hole [41, 42]. The merger of *two* second-generation black holes (2G+2G) is expected to be comparatively rare. For example, the fraction of second-generation and first-generation black hole mergers (2G+1G) in globular clusters can be more than one order of magnitude higher than 2G+2G mergers [42]. Taking selection effects into account, 2G+2G mergers could constitute at most 1% of all detected binary black hole mergers if black holes are born with non-negligible spin [42], as hinted by other analyses [14, 33]. The gap that we identify in the m_2 distribution may therefore represent the dearth of 2G+2G mergers. The prediction of 2G+2G rates in AGN is much more uncertain, replying on the details of gas-assisted migration.

Second-generation black holes are expected to merge with significant spins, inherited from the orbital angular momentum of their progenitor binaries. If they are indeed hierarchical mergers, we therefore expect the binaries with $m_1 \gtrsim 45 M_\odot$ to include a primary with dimensionless spin of $\chi_1 \approx 0.7$. Thus, measurements of black hole spin provide a means to independently verify our interpretation of a pair-instability mass gap contaminated with hierarchical mergers. Previous studies in GWTC-3 [18, 19] have shown a transition of spin properties of mergers; Ref. [18] first measured the transition at around the mass of $47^{+46}_{-10}\,M_\odot$ and Ref. [43] constrained that at $m_1 = 45^{+7}_{-5}\,M_\odot$ and associated that with the pair-instability gap. The spin distribution of the massive binary black holes is consistent with the prediction of hierarchical mergers. To this end, we reanalyse GWTC-4 using the mass-dependent spin model developed in Ref. [19]. In this model, the distribution of binary black-hole effective inspiral spin $\chi_{\rm eff}$

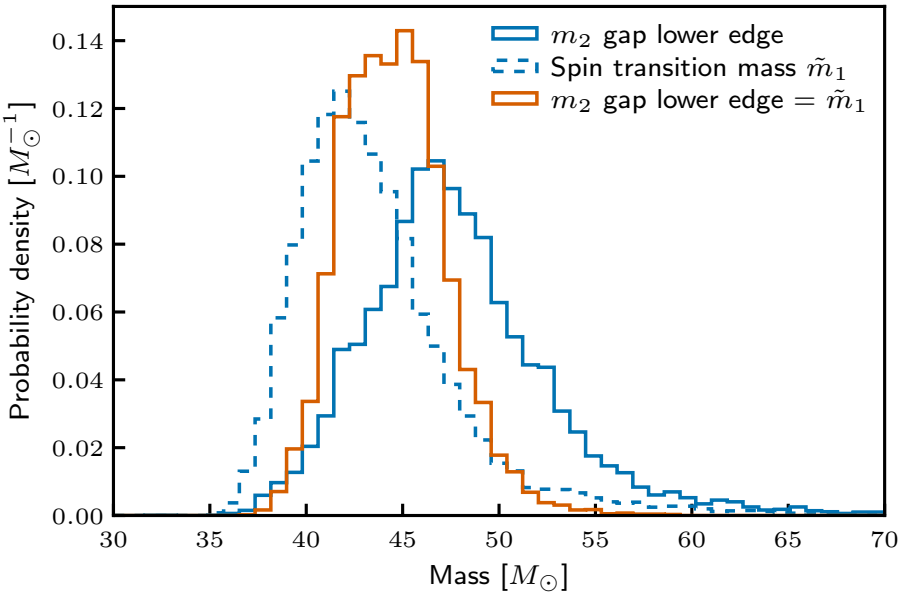

Fig. 2 Posterior for the lower edge of the mass gap as determined by different properties. We plot the posterior on the spin transition mass $\tilde{m}_1$ with dashed line in blue; see Equation (7) for the definition. We plot the posterior on the lower edge of the gap in m_2 with solid line in blue. Those two mass scales are independently but simultaneously inferred using the model allowing both m_2 gap and spin transition mass $\tilde{m}_1$. In orange, we plot the posterior on the mass scale when the lower edge of the m_2 mass gap is taken to be the same as $\tilde{m}_1$.

[1] differs depending on whether the primary mass is below or above some transition mass $\tilde{m}_1$ (See Section 1.6 for additional details). Given our astrophysical interpretation of the m_2 mass gap, we expect the spin transition mass $\tilde{m}_1$ to be consistent with the lower edge of the mass gap visible in m_2.

The results of this study are summarized in Fig. 2. We plot the posterior on the spin transition mass $\tilde{m}_1$ with dashed line in blue. It is strikingly consistent with the posterior on the lower edge of the m_2 mass gap, which is plotted with solid line in blue. We conclude that the distribution of black-hole masses and the distribution of black-hole spins provide concordant evidence for a pair-instability gap contaminated by 2G+1G hierarchical mergers. If we force the lower edge of the m_2 mass gap to be the same as $\tilde{m}_1$, we obtain the orange posterior, which implies a lower edge of $44^{+5}_{-4}\,M_\odot$. This model, in which the spin transition mass is fixed to the lower edge of

[1] The effective inspiral spin parameter,

$$\chi_{\rm eff} \equiv \frac{\cos(\mathrm{tilt}_1)\chi_1 + q\cos(\mathrm{tilt}_2)\chi_2}{1+q}, \tag{1}$$

is a weighted sum of the black hole spin from each component black hole. It is an approximate constant of motion [44].

the m_2 gap, is favoured over the transition-spin model without an m_2 gap by a $\ln \mathcal{B}$ of $\sim$3.3, and we adopt it for the remaining results unless otherwise specified.[2]

Using the inferred population distribution as a prior to inform the masses of individual events, Figure 3 shows the population-informed masses m_1 and m_2 for events in GWTC-4. Each event is colored by the posterior median of the absolute magnitude of its inspiral spin parameter $|\chi_{\rm eff}|$. We can see a clear gap in m_2 among the observed events, together with the transition from relativity small to large absolute values of effective spin happening around the same mass scale in m_1 as the lower edge of the gap in m_2. While hierarchical mergers in dense stellar clusters are usually predicted to have isotropic spin orientations due to dynamical assembly, preferentially aligned spins can arise from black holes in AGN disks or interactions between black holes and stars in clusters [e.g., 45]. In Section 1.7, we test the symmetry of the spin distribution for the high mass mergers and show it is consistent with being symmetric around zero, matching the prediction of 2G+1G mergers from dense stellar clusters well.

By assuming all mergers with m_1 inside the gap are 2G+1G hierarchical mergers, we infer a lower limit on the 2G+1G merger rate of $2.5^{+2.1}_{-1.3} \times 10^{-1}\mathrm{Gpc}^{-3}\,\mathrm{yr}^{-1}$. We also put an upper limit on the rate of mergers with both components in the gap $< 7.9 \times 10^{-2}\,\mathrm{Gpc}^{-3}\,\mathrm{yr}^{-1}$ at 90% credibility (see Section 1.3 for details). By checking for events with primary masses unambiguously in the mass gap and secondary masses below the gap, we can identify individual events that are likely to be 2G+1G hierarchical mergers. Using the population-informed masses, we calculate the Bayes factor $\mathcal{B}$ between the hypothesis that an event contains a black hole with primary mass inside the gap to the hypothesis that it does not. We find four events with strong support for the hierarchical-merger hypothesis ($\ln \mathcal{B} > 8$): GW190519_153544, GW190602_175927, GW191109_010717 and GW231102_071736. The exceptional event GW190521 (with total mass $150 M_\odot$) is conspicuously absent from this list. This is because it is consistent with the "straddling binary" hypothesis [46], where the primary mass exceeds the upper edge of the mass gap and the secondary mass falls below the lower edge, although it still has a $\ln \mathcal{B}$ of 1.7 in favour of the primary component in the gap (see Section 1.9 for additional details). We estimate the merger rate of such "straddling binaries" with one component from the far side of the gap and the other component below the gap to be $5.8^{+16.6}_{-4.6} \times 10^{-3}\,\mathrm{Gpc}^{-3}\,\mathrm{yr}^{-1}$. Meanwhile, the rate of mergers with both components on the far side of the gap is $3.8^{+4.6}_{-2.2} \times 10^{-2}\,\mathrm{Gpc}^{-3}\,\mathrm{yr}^{-1}$. Assuming a GWTC-4 cumulative search sensitivity, we expect 53^{+25}_{-20} in 300 binary black hole events to have primary masses in the gap and secondary masses below the gap. Meanwhile, we infer 6^{+7}_{-5} in 300 binary black hole events to contain at least one component on the far side of the gap, out of which 0^{+3}_{-0} can be straddling binaries. Under our best model, which indicates zero detections of binaries with both components in the mass gap, the Poisson counting uncertainty implies a 90% upper limit of $\lesssim 4.5$ such systems in a catalog of 300 binary black hole detections.

[2] As Ref. [19] showed, the transition-spin model (without an m_2 gap) is strongly favoured over a model in which the entire population is represented by a single Gaussian in $\chi_{\rm eff}$ by $\ln \mathcal{B} > 9$. Our fiducial model, in which the spin transition mass is equal to the lower edge of the m_2 gap, is further favoured over Ref. [19]'s model ($\ln \mathcal{B} \sim 3.3$), as well as a model in which the spin transition mass can be different from the lower edge of the m_2 gap ($\ln \mathcal{B} \sim 1.0$).

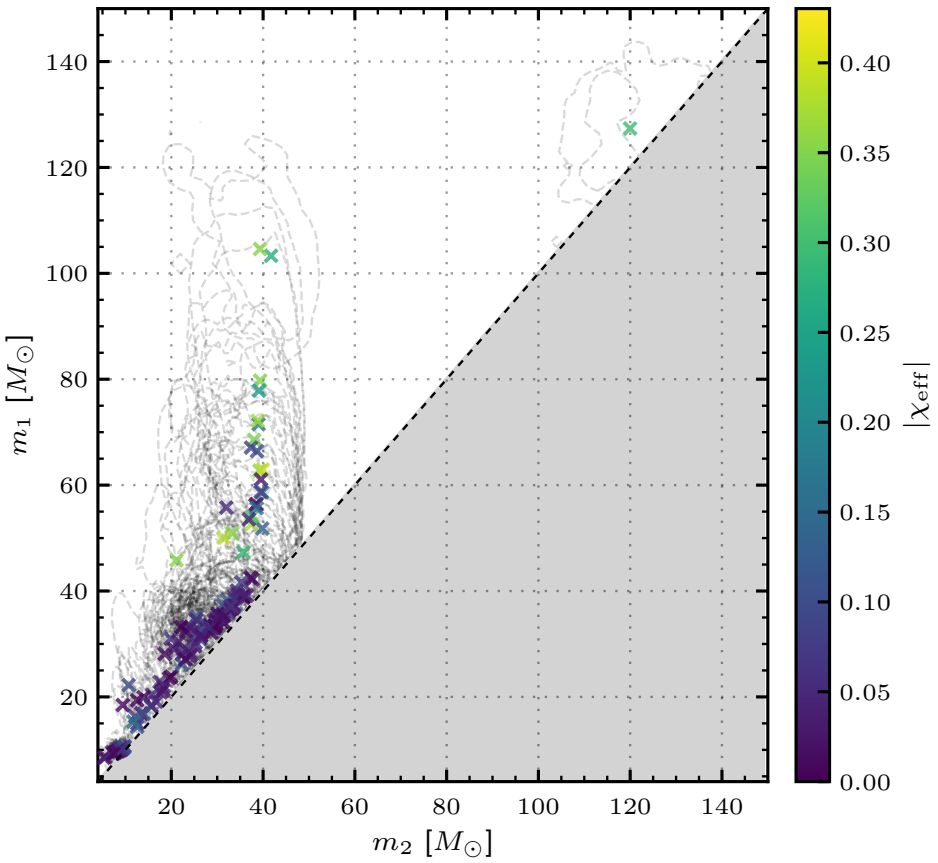

Fig. 3 Primary masses m_1 and secondary masses m_2 coloured according to $\chi_{\rm eff}$ for GWTC-4 events, where the masses of each event are simultaneously inferred with the population. We fit the population to a model that allows for a gap in m_2 and a $\chi_{\rm eff}$ spin distribution that transitions at the lower edge of the m_2 gap. Crosses show the median values of m_1 and m_2. Contours show 90% credible intervals.

The location of the pair-instability gap measurement can be used to constrain the $^{12}\mathrm{C}(\alpha,\gamma)^{16}\mathrm{O}$ rate [7, 13, 23]. In astrophysics, the reaction cross section is commonly described by the S-factor, which is the nuclear structure-dependent part of the cross section for charged-particle nuclear reactions—isolated from Coulomb repulsion. Based on simulations, Ref. [13] fit the lower edge of the mass gap as a function of the temperature-dependent uncertainty in the $^{12}\mathrm{C}(\alpha,\gamma)^{16}\mathrm{O}$ rate and reported constraints on the $^{12}\mathrm{C}(\alpha,\gamma)^{16}\mathrm{O}$ using the first ten gravitational-wave detections. However, in order to determine the lower edge of the mass gap with so few events, the analysis had to employ a model with rather strong assumptions about the shape of the black hole mass distribution. Following the observation of additional binary black hole signals, it became apparent that this early model was misspecified, and so the earliest inferences on the lower edge of the mass gap were unreliable [14, 21]. A more recent analysis

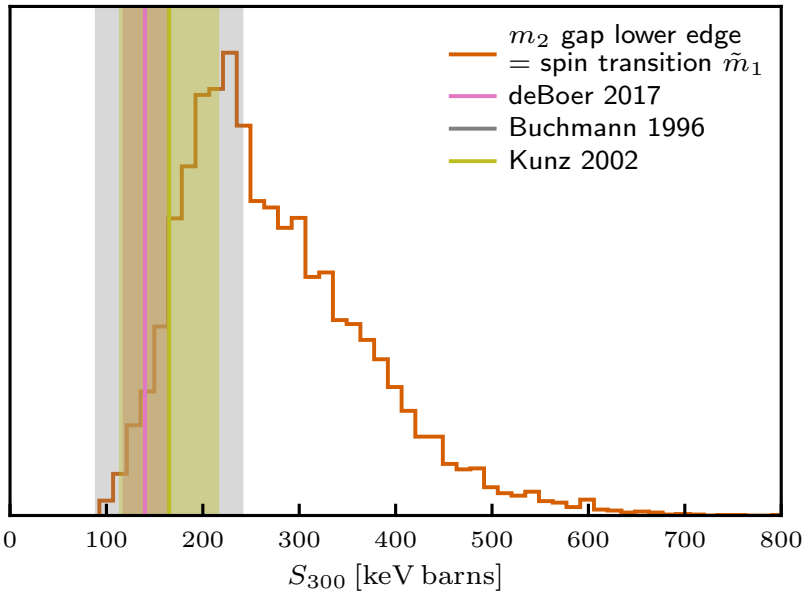

Fig. 4 Constraints on $^{12}\mathrm{C}(\alpha,\gamma)^{16}\mathrm{O}$ rate. Orange is the posterior using the measurement imposing lower edge of the m_2 gap equal to the spin transition mass $\tilde{m}_1$. Pink shows the theoretical nuclear physics prediction from Ref. [47] of 140^{+21}_{-21} keV barns (68% credibility). Grey shows the result from Ref. [48] of 165^{+75}_{-75} keV barns (68% credibility) and yellow-green shows the result from Ref. [49] of 165^{+50}_{-50} keV barns (68% credibility).

[23] explored the possibility of the bump around $35\,M_\odot$ in binary black hole mass distribution to be a signature from the pulsational pair-instability process and found the inferred astrophysical S-factor in tension with Ref. [47], illustrating the difficulty of placing constraints on $^{12}\mathrm{C}(\alpha,\gamma)^{16}\mathrm{O}$ reaction rates using previous gravitational-wave catalogues. Using the relationship between the lower edge of the mass gap and the $^{12}\mathrm{C}(\alpha,\gamma)^{16}\mathrm{O}$ rate fit from Ref. [13], we constrain the astrophysical S-factor of $^{12}\mathrm{C}(\alpha,\gamma)^{16}\mathrm{O}$ at 300 keV to 260^{+190}_{-108} keV barns (90% credibility), as seen in Fig. 4. Our constraint on the S-factor is consistent with that of Ref. [47] with the median prediction of Ref. [47] within the 93% credible interval, though our posterior favours higher values. A higher S-factor is more consistent with the values reported, e.g., in Refs. [48–50]. However, we do not interpret our result to be in tension with Ref. [47]. Since the mapping from the lower edge of the gap to the corresponding S-factor is non-linear, small shifts towards a lower inferred edge lead to a long tail towards higher inferred S-factors. We show in Sec. 1.8 that shifting the lower edge by $\sim 2\,M_\odot$ results in a S-factor estimate that aligns well with the result of Ref. [47] (see the blue curve of Extended Fig. 9). Moreover, the simulations mapping from the gap to the corresponding $^{12}\mathrm{C}(\alpha,\gamma)^{16}\mathrm{O}$ rate in Ref. [13] simulated the lowest edge $\sim 40M_\odot$ while our constraint has an error bar extending to $< 40M_\odot$. Thus, the long tail to high S-factors in our posterior may be unrealistic.

Going forward, it is important to include the m_2 gap in binary black hole population models if this feature remains consistent with pair-instability theory. The presence of a gap in the distribution of black hole masses can be used to break the degeneracy between distance and redshift, facilitating measurements of the Hubble parameter [51]. Since the location of the pair-instability gap is predicted to evolve only minimally with cosmic time [34], it may provide a more robust feature for cosmological inference than the $35\,M_\odot$ bump [22], whose physical origin is unknown. While we interpret the dearth of binary black holes with $m_2 \gtrsim 45M_\odot$ as evidence of a pair instability gap—and while we regard this explanation as a promising and plausible explanation—we acknowledge that the data are open to other interpretations. For example, one could imagine that a dearth of events with $m_2 \gtrsim 45M_\odot$ might be produced through the complicated interplay between the initial stellar mass function and binary interactions, thereby mimicking a pair instability gap through unrelated physical processes. If subsequent data continue to show a gap for binaries with $m_2 \gtrsim 45M_\odot$ regardless of the mass of the primary black hole, alternative explanations of the gap invoking binary interactions may begin to appear contrived. More excitingly, future measurements of spin orientations may help indicate the evolutionary pathways and formation environments of high-spin events to further test the hierarchical merger hypothesis.

1 Methods

1.1 Hierarchical Bayesian inference details

We perform hierarhical Bayesian inference with `GWPopulation` [52] on the recently released cumulative Gravitational Wave Transient Catalog 4 [32, 53–57]. There are roughly 80 confident binary black holes detected in the first part of the LIGO–Virgo–KAGRA's fourth observing run (O4a), enabled by a variety of detector improvements [58–62]. Our dataset includes 153 binary black holes with false-alarm rates $\leq 1\,\mathrm{yr}^{-1}$, consistent with Ref. [33]. Selection effects are taken into account by a Monte Carlo estimation [63–66]. We use the posterior samples consistent with the choice of Ref. [33], generated using `Bilby` and `Dynesty` [67–69]. For events detected before O4a, we use the MIXED samples reported in GWTC-3 and GWTC-2.1 [38, 70].

As the previously known event with the highest support for pair-instability gap components GW190521, Ref.[71] concluded the NRSur7dq4 waveform model is most faithful to NR simulations in the parameter range relevant for this exceptional event. We tested different waveform models for this event and concluded the results of our pair-instability gap measurement are not sensitive to the choice of waveform. Using NRSur7dq4 posterior samples of GW19021, we found the lower edge of 49^{+10}_{-6} from mass distribution and 45^{+5}_{-3} by incorporating spin transition information.

1.2 Basic mass gap model

To model the predicted pair-instability gap [1–7, 34, 72], we employ an extension of the basic binary black-hole mass models in Ref. [33]. The mass model is parameterized via source-frame primary mass m_1 and secondary mass $m_2 < m_1$, so we are fitting

the distribution

$$\pi(m_1, m_2|\Lambda) = \pi(m_1|\Lambda)\,\pi(m_2|m_1, \Lambda), \tag{2}$$

which is conditioned on hyper-parameters Λ that control the shape of the distribution. As discussed below, we employ various models for $\pi(m_1|\Lambda)$ from Ref. [33]. The key ingredient, however, is our model for secondary mass, which enforces a gap in the distribution of m_2:

$$\pi(m_2|m_1, \Lambda) \propto \begin{cases} 0 & m_g \leq m_2 \leq m_g + w_g\,, \\ m_2^{\beta_q} & \text{otherwise}\,. \end{cases} \tag{3}$$

Here, m_g is the lower boundary of the m_2 mass gap and w_g is the width of the gap. We assume a Bayesian prior on m_g that is uniform on the interval $(20M_\odot, 150M_\odot)$ while w_g is uniform on the interval $(0M_\odot, 150M_\odot)$. This model implies that the secondary mass is a power-law distribution unless m_2 is on the interval $(m_g, m_g + w_g)$ where no mergers are allowed.

We perform the analysis using the Broken Power Law + Two Peaks model for $\pi(m_1)$ from Ref. [33]. In order to investigate the dependence of our results on this model, we then repeat the analysis using the Single Power Law + Two Peaks model from Ref. [33]. For our initial analysis—before we model the spin transition mass from Ref. [19] (below)—we employ the default spin model from Ref. [33], which consists of independent and identical truncated Gaussian distributions for the spin magnitudes of the primary and secondary black holes. Meanwhile, the cosine of the spin tilt distribution is modeled as a mixture of a uniform distribution and a Gaussian distribution with free mean and width. The evolution of the merger rate over redshift is modelled as a power-law distribution [21, 53].

While Broken Power Law + Two Peaks model is found to be the statistically favoured in Ref. [33], the break mass is not constrained at all when we introduce the flexibility of a gap in m_2 distribution. The slopes of the two bands of the broken power law distribution are consistent with each other. We interpret the initial requirement of a second power law in the m_1 distribution in current data as a projection of the dearth of high m_2 events. Instead, we find that the Single Power Law + Two Peaks model has the highest Bayesian evidence when we allow for a gap in the secondary mass distribution. When we employ the Broken Power Law + Two Peaks model, the existence of the m_2 mass gap in the model is preferred over the no-gap model by a $\ln \mathcal{B}$ of $\sim$3.7. Using the Single Power Law + Two Peaks model, the model with a gap is preferred with $\sim$84. The plots in this paper use our best mass model, Single Power Law + Two Peaks with a gap, unless otherwise stated. We summarize the model comparison result in Table 1.

Extended Fig. 1 shows the posterior distribution for the lower edge of the gap m_g and the upper edge of the gap $m_g + w_g$. The results from GWTC-4, including the exceptionally massive event GW231123 [35], are shown in blue. The inclusion of GW231123 is necessary in order to obtain a useful constraint on the upper edge of the gap. However, as noted before, the large spins of GW231123 may suggest that it

Model	$\ln \mathcal{B}$	Relative maximum $\ln \mathcal{L}$
Broken Power Law + Two Peaks without m_2 gap	1	0
Single Power Law + Two Peaks with m_2 gap	4.4	8.84
Broken Power Law + Two Peaks with m_2 gap	3.7	9.23
Single Power Law + Two Peaks with m_2 notch filter	1.8	6.98
Single Power Law + Two Peaks with m_2 notch filter (A=1)	4.4	-

Table 1 The natural logarithm Bayes factor and maximum likelihood comparison of a few variations of the basic mass model with the default model of Ref [33] as the baseline. The Bayes factor of Single Power Law + Two Peaks with m_2 notch filter model assuming $A = 1$ (i.e., empty gap case) is approximated by the Savage-Dickey density ratio.

is a contamination-event from a 2G+2G merger as opposed to a binary with black holes formed above the pair instability gap. The constraints on the m_g obtained without GW231123 (orange) are not significantly different from the results obtained with GW231123. The results obtained from GWTC-3 [38] are consistent with results from GWTC-4, albeit with decreased statistical significance.

We perform a posterior predictive check. The distribution predicted by our mass-gap model is consistent with the observed gravitational-wave events, as shown in Extended Fig. 2. The cumulative density of secondary masses m_2 reaches a plateau around the lower edge of the gap $\sim 45\,M_\odot$ until $\sim 116\,M_\odot$ with a tiny bump for both the observed and predicted distributions due to the mergers at the far end of the gap.

1.3 Gap depth investigation with a notch-filter model

We replace the model of a fixed empty gap in Eq. (3) by a notch filter $n(m_2)$ to investigate the depth of the gap:

$$\pi(q|\Lambda) \propto q^{\beta_q} n(m_2). \tag{4}$$

The expression for the notch filter can be written as [73]

$$n(m_2) = 1 - \frac{A}{(1 + (\frac{m_g}{m_2})^{\eta_{\rm low}})(1 + (\frac{m_2}{m_g + w_g})^{\eta_{\rm high}})}, \tag{5}$$

where m_g and w_g are hyper-parameters describing the lower edge and the width of the gap, $\eta_{\rm low}$ and $\eta_{\rm high}$ set the sharpness of the gap's edges, and the amplitude of the gap is determined by the parameter A. We choose the same priors for m_g and w_g as our standard gap model. We employ uniform priors on A in range of [0,1] as well as $\eta_{\rm low}$ and $\eta_{\rm high}$ in range of [0,50]. Higher values of $\eta_{\rm low}$ and $\eta_{\rm high}$ corresponds to sharp low and high edges respectively.

We show the posteriors of those parameters in Extended Fig. 3. The posterior of A is sharply peaked at 1, which represents the preference of an empty gap with the lower edge of the gap consistent with our default model result. The inference of the upper edge in this notch filter model is much more uncertain given a more flexible description of the gap, which is expected since it is mostly driven by the detection of a single event. Non-sharp edges are disfavoured, in particularly for the lower end, and

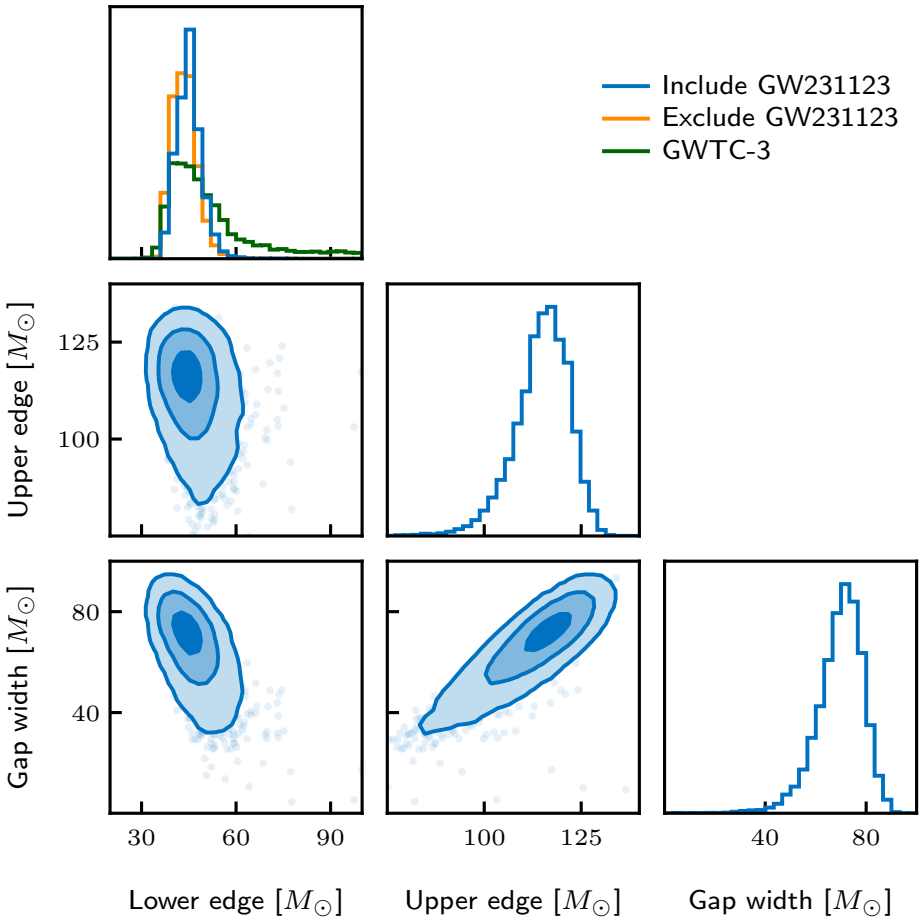

Extended Figure 1 Corner plot of the lower, upper boundary and the width of the secondary mass gap. The results from GWTC-4 including the exceptionally massive event GW231123 are shown in blue. This event is necessary to obtain a useful constraint on the upper edge of the mass gap. Constraints on the lower edge obtained with GWTC-4 excluding GW231123 (orange) and with GWTC-3 (green) are made by inferring the maximum truncation in the m_2 distribution. The constraints on the lower edge excluding GW231123 are consistent with those obtained with GW231123.

increasing sharpnesses are not distinguishable (also from a hard cutoff) given current dataset.

With the flexibility of a finite depth of the gap in this model, we can also place an upper limit on the rate of BBHs that have both components inside the gap by the non-detection of such events. Assuming that any component inside the gap is a 2G black hole, we place constraints on the upper limit of the merger rates of 2G+2G black holes in the gap to be $< 7.9 \times 10^{-2}\,\mathrm{Gpc}^{-3}\,\mathrm{yr}^{-1}$ at 90% credibility.

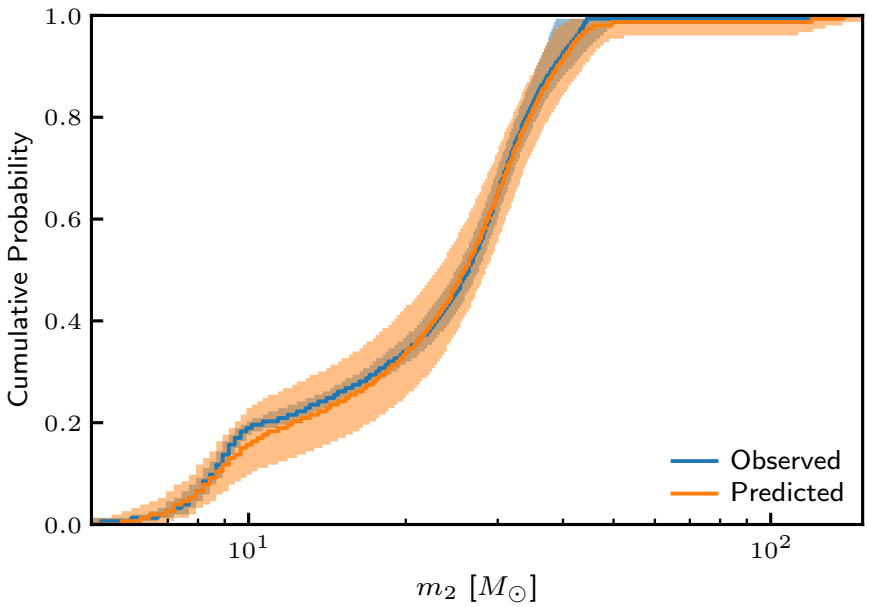

Extended Figure 2 A posterior predictive check: the cumulative function of the observed events' secondary-mass distribution (blue) versus the predicted secondary-mass distribution for the SINGLE POWER LAW + TWO PEAKS model with a gap in m_2 (orange). The solid lines indicate the median and the shaded bands indicate the 90% credibility range.

1.4 Comparison to the maximum population likelihood distribution

The π formalism introduced in Ref. [37] offers a data-driven approach to visualizing the population properties of merging binaries.[3] Rather than fitting a model, the π formalism identifies the unique distribution that maximizes the population likelihood over all possible population models. The resulting distribution $\pi(\theta)$ is always given by a weighted sum of delta functions, with the locations and weights of the "π samples" are determined via constrained numerical optimization. The samples show which population features are supported by the data, as opposed to features that might be inferred due to model-dependence. In the limit where the number of observations goes to infinity, the π samples reproduce the true distribution [37].

Extended Fig. 4 shows π in (m_1, m_2) for the data in GWTC-4. The background contour shows the probability density inferred by the standard parametric model, SINGLE POWER LAW + TWO PEAKS with m_2 gap. The π samples are consistent with our fit; there is a notable absence of π samples with secondary mass between approximately $45\,M_\odot$ and $116\,M_\odot$. The π gap is not imposed by any modelling assumptions, but rather emerges organically from the data. The agreement between the model-free π distribution and the parametric model analysis gives us additional confidence in the

[3] The symbol π is pronounced "pi stroke."

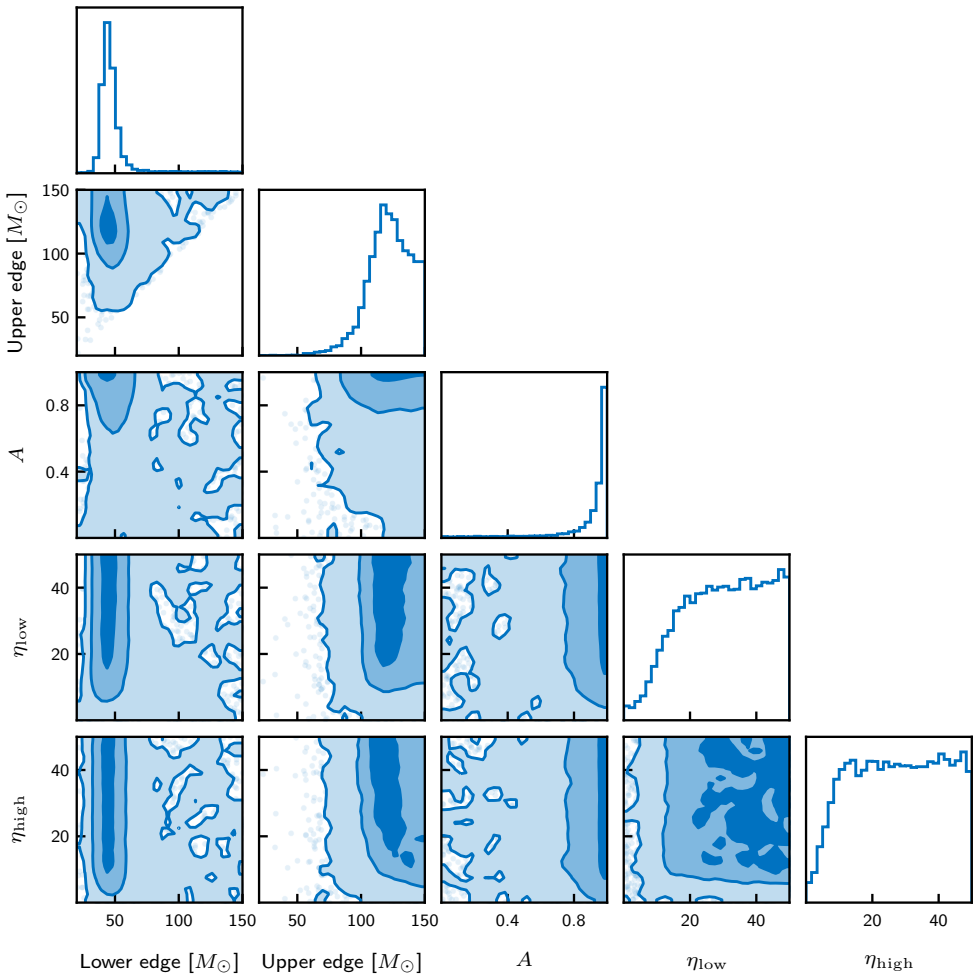

Extended Figure 3 Corner plot of the notch filter parameters.

existence of a pair-instability mass gap in the distribution of secondary component masses.

1.5 Mass model misspecification test

As a further test of model misspecification, we also run the analysis using the pairing mass model from Ref. [74]. In this model, the joint distribution for m_1 and m_2 is written as

$$\pi(m_1, m_2) \propto \pi(m_1|\Lambda_1)\,\pi(m_2|\Lambda_2)\,f(q|\beta_q). \tag{6}$$

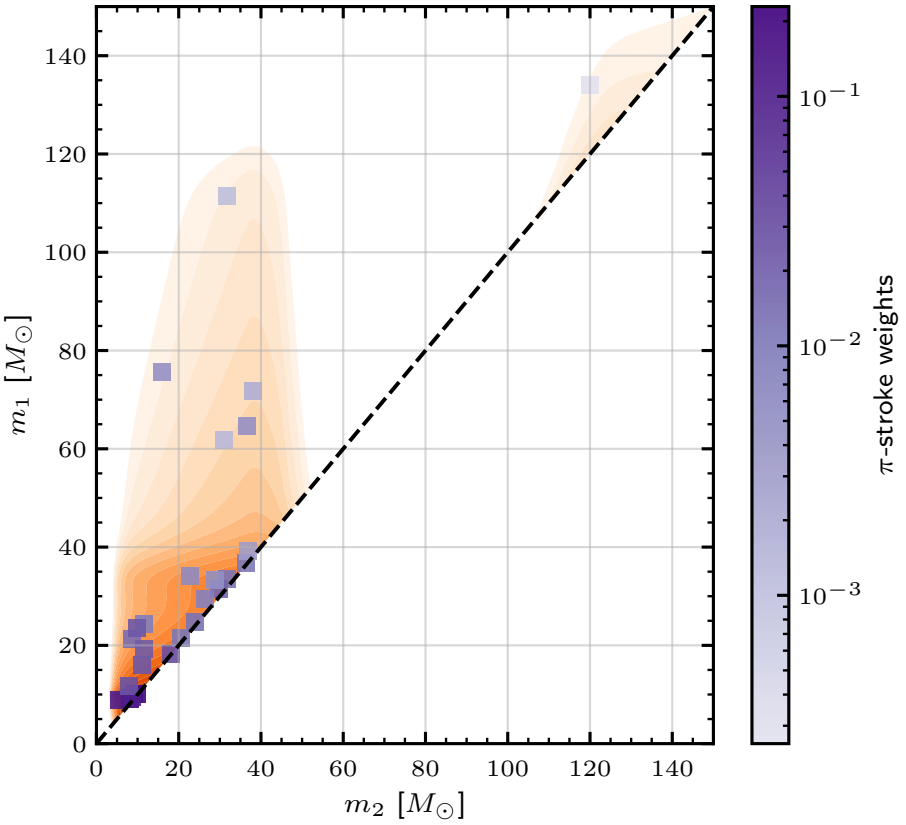

Extended Figure 4 Predicted population distribution by maximum population likelihood method, the π-stroke ($\pi\!\!\!-$) formalism. The distribution is expressed as a weighted sum of delta functions. Scatter points show where the delta functions are in terms of (m_1, m_2). The colorbar represents the weights of delta functions. We also show the mean prediction of the joint distribution $\pi(m_1, m_2)$ by our standard parametric model analysis in the background for reference. Both analyses show consistent support for m_2 gap.

The hyper-parameters Λ_1 control the shape of a nominal[4] distribution for primary mass while the hyper-parameters Λ_2 control the shape of a nominal distribution of secondary mass. The pairing function $f(q|\beta_q)$ is a power law in mass ratio $q = m_2/m_1$. With more parameters than our Single Power Law + Two Peaks model, this pairing mass model provides significantly more flexibility to reconstruct distributions in the m_1–m_2 plane.

In our version of the pairing mass model, we employ separate Broken Power Law + Two Peaks models for $\pi(m_1|\Lambda_1)$ and $\pi(m_2|\Lambda_2)$. For the sake of simplicity

[4]We use the word "nominal" here because the marginal distribution $\int dm_2\, \pi(m_1, m_2)$ is not equal to $\pi(m_1|\Lambda_2)$.

of a test focusing on the lower edge of the gap, we exclude GW231123. We additionally allow for the presence of different maximum truncation for m_1 and m_2. The reconstructed distributions are shown in Extended Fig. 5. Interestingly, the pairing mass model does not require hard cutoff in the m_2 distribution around $45M_\odot$. This is because it can produce a dearth of events with $m_2 \gtrsim 45M_\odot$ with a steeply falling power law. This is evidenced by comparing upper quantiles for the pairing mass and Single Power Law + Two Peaks mass models. In Extended Fig. 6, we plot the 99th percentile $m_2^{99\%}$ of secondary masses in the population. The two distributions from Single Power Law + Two Peaks model and the pairing mass model agree. Repeating this exercise for the 99.9% quantile (dashed), we see the two distributions again agree. We conclude that the pairing mass model fit is *functionally equivalent* to one with a hard cutoff in m_2, even though this can be achieved without an explicit cutoff. The difference in $m_1 > 175M_\odot$ region between the models is caused by a fixed maximum $m_1 = 300M_\odot$ truncation in our Single Power Law + Two Peaks model following the setup of Ref. [33]. However, the maximum m_1 truncation is not constrained at all when it is analysed as a free parameter. The choice of a fixed maximum m_1 truncation makes no difference in the inference of other major structures of the mass distribution.

1.6 Spin transition study

Next, we replace the default spin model with the model from Ref. [19], which showed evidence for a change in the spin distribution for primary masses above $\tilde{m}_1$. We consider two model variations. In the first variation, the effective inspiral spin parameter $\chi_{\rm eff}$ is normally distributed when $m_1 < \tilde{m}_1$ and it is uniformly distributed when $m_1 > \tilde{m}_1$ [19]:

$$\pi(\chi_{\rm eff}|m_1,\Lambda) = \begin{cases} \mathcal{N}(\chi_{\rm eff}|\mu,\sigma) & (m_1 < \tilde{m}_1) \\ \mathcal{U}(\chi_{\rm eff}|w=0.47) & (m_1 \geq \tilde{m}_1). \end{cases} \tag{7}$$

The second variation employs a mixture model for binaries with $m_1 > \tilde{m}_1$[19]:

$$\pi(\chi_{\rm eff}|m_1,\Lambda) = \begin{cases} \mathcal{N}(\chi_{\rm eff}|\mu,\sigma) & (m_1 < \tilde{m}_1) \\ \zeta\,\mathcal{U}(\chi_{\rm eff}|w) + (1-\zeta)\mathcal{N}_{\rm u}(\chi_{\rm eff}|\mu_{\rm u},\sigma_{\rm u}) & (m_1 \geq \tilde{m}_1). \end{cases} \tag{8}$$

We show in Extended Fig. 7 that both models produce similar results. However, the complexity of Eq. (8) means this model is disfavoured due to an Occam penalty. We therefore report our results using the spin model Eq. (7) throughout the paper, unless otherwise specified.

Ref. [75] further investigates this spin transition feature using a non-parametric model for the spin distribution of the high mass sub-population. It is shown that with a weaker assumption on the spin model, the measurement of the spin transition mass $\tilde{m}_1$ is still consistent with the results using the parametric models introduced above.

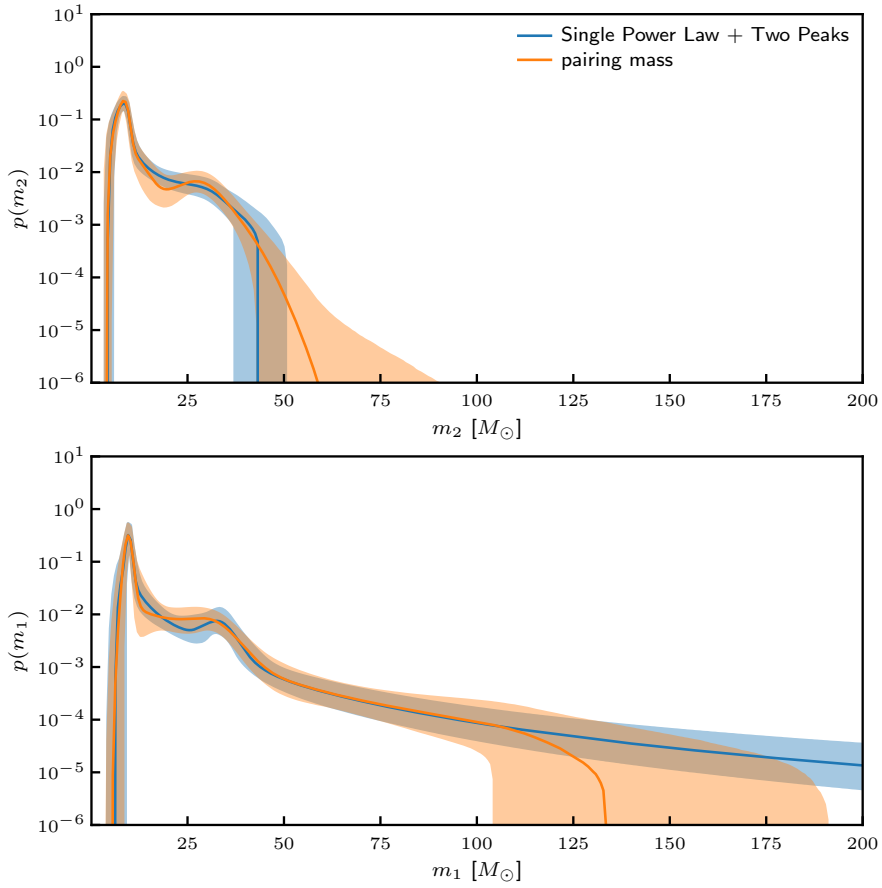

Extended Figure 5 Reconstructed distributions of primary masses m_1 (top) and secondary masses m_2 (bottom). The blue fit is obtained with the SINGLE POWER LAW + TWO PEAKS model while the orange fit is obtained with the pairing mass model from Ref. [74].

1.7 Symmetry of the effective spin distribution for the high mass mergers

We explore whether the spin distribution for the high mass mergers is isotropic or not by a more flexible model following [43, 75]. We extend model in Eq. 7 to allow the minimum and maximum truncation of the uniform distribution which describes the

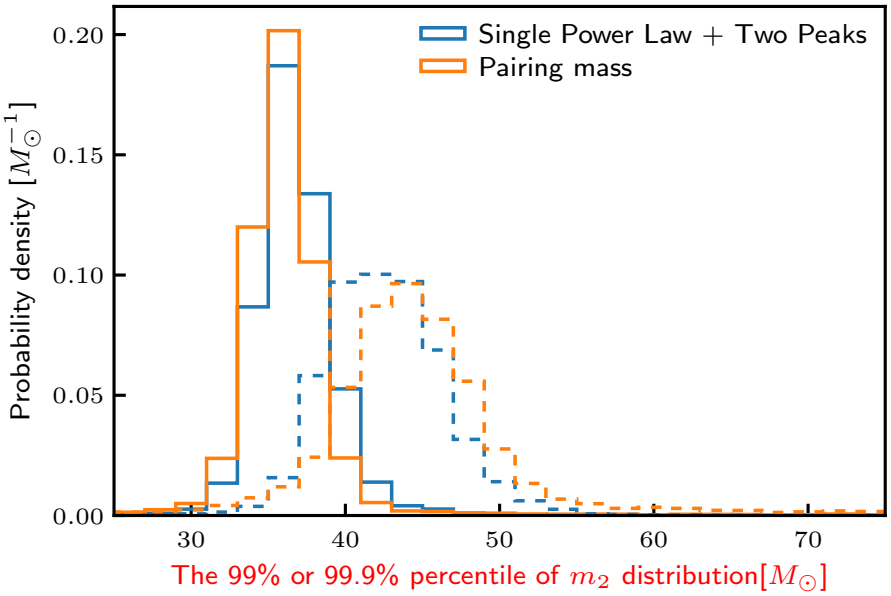

Extended Figure 6 Comparing quantiles for different models: 99% of mergers are below $m_2^{99\%}$ (solid) and 99.9% are below $m_2^{99.9\%}$ (dashed-dotted). Blue shows the results for the SINGLE POWER LAW + TWO PEAK model while orange shows the results for the more flexible pairing mass model[74].

spin distribution for the high mass mergers to be free parameters.

$$\pi(\chi_{\rm eff}|m_1,\Lambda) = \begin{cases} \mathcal{N}(\chi_{\rm eff}|\mu,\sigma) & (m_1 < \tilde{m}_1) \\ \mathcal{U}(\chi_{\rm eff}|\chi_{\rm min}^{\text{high-mass}},\chi_{\rm max}^{\text{high-mass}}) & (m_1 \geq \tilde{m}_1). \end{cases} \tag{9}$$

We set the prior for $\chi_{\rm min}^{\text{high-mass}}$ that is uniform on the interval $(-1,1)$ and $\chi_{\rm max}^{\text{high-mass}}$ that is uniform on the interval $(-1,1)$.

We show the result of the spin distribution for high mass mergers in extended Fig. 8. While the lower boundary of the spin distribution is relatively less constrained than the upper boundary, the overall distribution is consistent with a spin distribution symmetric around zero. We found the mean $\langle\chi_{\rm eff}\rangle = ((\chi_{\rm max}^{\text{high-mass}} + \chi_{\rm min}^{\text{high-mass}})/2 = -0.00^{+0.12}_{-0.10}$ and the half-width $\mathrm{w}^{\chi}_{\rm high-mass} = ((\chi_{\rm max}^{\text{high-mass}} - \chi_{\rm min}^{\text{high-mass}})/2 = 0.53^{+0.12}_{-0.15}$. A positive minimum truncation, $\chi_{\rm min}^{\text{high-mass}} > 0$, is ruled out at 99.3% credibility.

1.8 Constraints on the $^{12}\mathrm{C}(\alpha,\gamma)^{16}\mathrm{O}$ rate with different models

We show the constraints on the $^{12}\mathrm{C}(\alpha,\gamma)^{16}\mathrm{O}$ rate with other model assumptions in addition to the one in the main body of the paper. As mentioned, we used the relationship between the lower edge of the mass gap and the $^{12}\mathrm{C}(\alpha,\gamma)^{16}\mathrm{O}$ rate fit from Ref. [13].

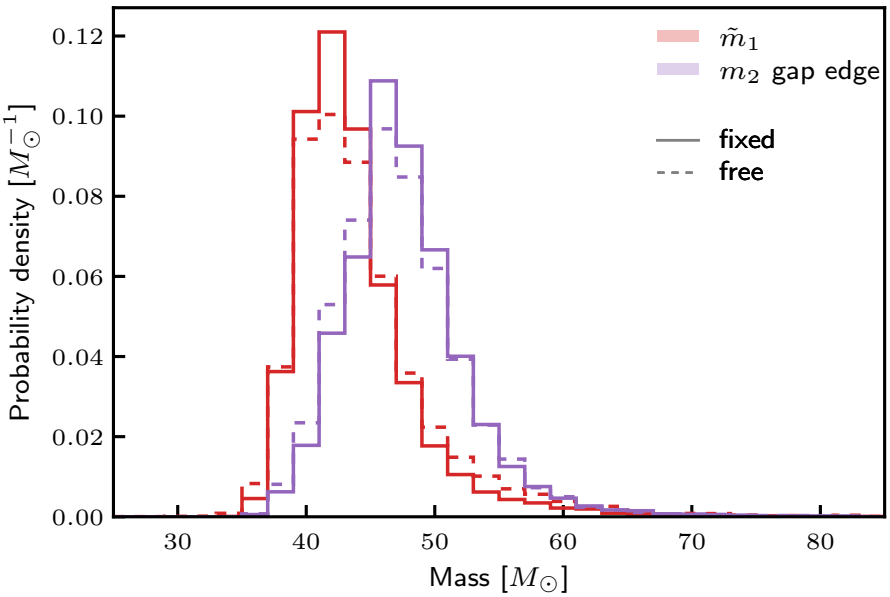

Extended Figure 7 Comparing the lower edge of the mass gap and the spin transition mass results using different spin models. We show the results in solid lines assuming the "simple" spin transition model from Eq. (7) while the results in dashed-dotted assume the more complicated spin transition model from Eq. (8). In purple is the posterior for the lower edge of the m_2 mass gap. Red shows the posterior for the spin transition mass $\tilde{m}_1$. The results are consistent between different spin transition models.

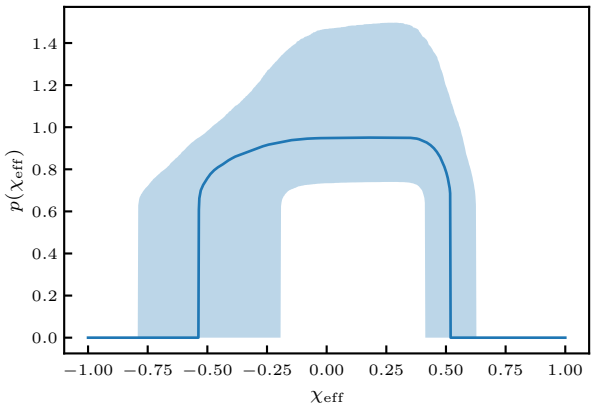

Extended Figure 8 The effective spin distribution for high mass binary black holes with $m_1 > \tilde{m}_1$ using the flexible spin model in Eq. 9. The shaded area represents the 90% credible interval and the solid line is the median.

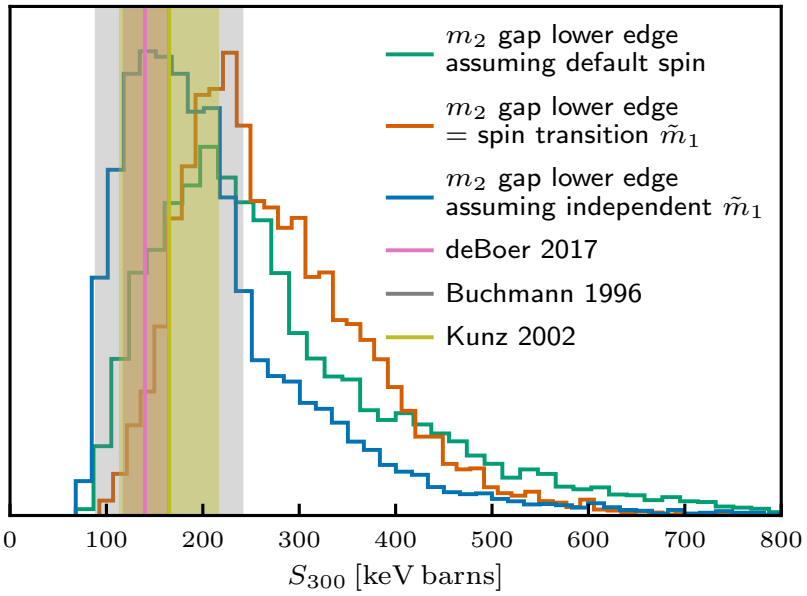

Extended Figure 9 Constraints on $^{12}\mathrm{C}(\alpha,\gamma)^{16}\mathrm{O}$ rate. Green is the posterior for S_{300} using the lower edge of the mass gap inferred assuming default spin model in Ref. [33]. Blue uses the measurement of the lower edge of the mass gap assuming the spin transition model in Ref. [19] while the spin transition mass $\tilde{m}_1$ is independent and non-identical of the m_2 gap. Orange is the posterior using the measurement imposing lower edge of the m_2 gap equal to the spin transition mass $\tilde{m}_1$. Results in pink, grey and and yellow-green show the theoretical nuclear physics predictions from Refs. [47–49].

As shown in Extended Fig. 9, we constrain the astrophysical S-factor of $^{12}\mathrm{C}(\alpha,\gamma)^{16}\mathrm{O}$ at 300 keV to 243^{+331}_{-119} keV barns (90% credibility) by mass gap measurement assuming default spin model and to 260^{+190}_{-108} keV barns (90% credibility) by incorporating spin transition information. In blue we also show the constraint at 186^{+282}_{-88} keV barns by the mass gap measurement while assuming a spin transition mass non-identical and independent of the m_2 gap. The measurements of the mass gap shift slightly given different assumptions on spin models due to the degeneracy, which leads to different but consistent posteriors of the astrophysical S-factor.

1.9 Implications for GW190521

The presence of an apparent gap due to pair-instability supernovae has interesting implications for previously identified gravitational-wave events with exceptional properties. GW190521 was highlighted as a potential candidate of hierarchical mergers in the mass gap [71, 76]. While this interpretation is consistent with our results, we also find support for the hypothesis—first put forward in Ref. [46]—that GW190521 is a straddling binary with component black holes on either side of the gap. We show a corner plot for the mass and spin properties of GW190521 in Extended Fig. 10. Within

the context of our population model, the secondary black hole in GW190521 is most likely below the pair instability gap: $m_2 = 40.7^{+8.9}_{-7.0}\,M_\odot$ at 90% credibility, though there is still marginal support for m_2 at the other end of the gap $\sim$120 $M_\odot$. There is posterior support $\sim 4\%$ for the hypothesis that both components of GW190521 are on the far side of the gap. Excluding GW231123, the overall population has a maximum $m_2 \sim 43\,M_\odot$ as shown in orange in our Extended Fig. 1. Thus the event GW190521 in this case is fully consistent with its secondary component below the gap.

For future work, we envision a global fit using a model that includes subpopulations of 1G+1G, 2G+1G and 2G+2G mergers; see, e.g., Refs. [16, 17, 77–79]. By explicitly modeling the 2G+1G subpopulation, it would be possible to account for contamination from hierarchical mergers in the m_1 mass gap. As the number of detections increases, it will be possible to gain new insights into the pair-instability gap and the prevalence of hierarchical mergers in merging binaries.

Data Availability. Results of the analyses in this work can be found on Zenodo[80]. The posterior samples of GWTC-4 events used in the hierarchical Bayesian inference of this work are available on Zenodo: 16053484 as part of LIGO-Virgo-Kagra's GWTC-4 data release [81]. For events in GWTC-2.1 and GWTC-3, we use samples from Zenodo: 6513631 and Zenodo: 554666 [82, 83]. We use the cumulative search sensitivity file on Zenodo: 16740128 [84].

Code Availability.

The code for this study is publicly available at https://github.com/HuiTong5/PISN_mass_gap_GWTC-4 as an implementation of the population models developed in this study using `GWPopulation` [52].

Acknowledgements We thank Zoheyr Doctor for inspiring this study. We thank Simon Stevenson, Christopher Berry, Thomas Dent, Anjali Yelikar, Parthapratim Mahapatra, Isobel Romero-Shaw, Fabio Antonini, Elenna Capote and Vaibhav Tiwari for comments. H.T. and E.T. are supported by the Australian Research Council CE230100016, LE210100002, DP230103088. M.F. acknowledges support from the Natural Sciences and Engineering Research Council of Canada (NSERC) under grant RGPIN-2023-05511, the University of Toronto Connaught Fund, the Alfred P. Sloan Foundation, and the Ontario Early Researcher Award. M.M. is supported by the LIGO Laboratory through the National Science Foundation awards PHY-1764464 and PHY-2309200.

This material is based upon work supported by NSF's LIGO Laboratory which is a major facility fully funded by the National Science Foundation. The authors are grateful for for computational resources provided by the LIGO Laboratory computing cluster at California Institute of Technology supported by National Science Foundation Grants PHY-0757058 and PHY-0823459. LIGO was constructed by the California Institute of Technology and Massachusetts Institute of Technology with funding from the National Science Foundation and operates under cooperative agreement PHY-1764464. This paper carries LIGO Document Number LIGO-P2500453.

Author contributions

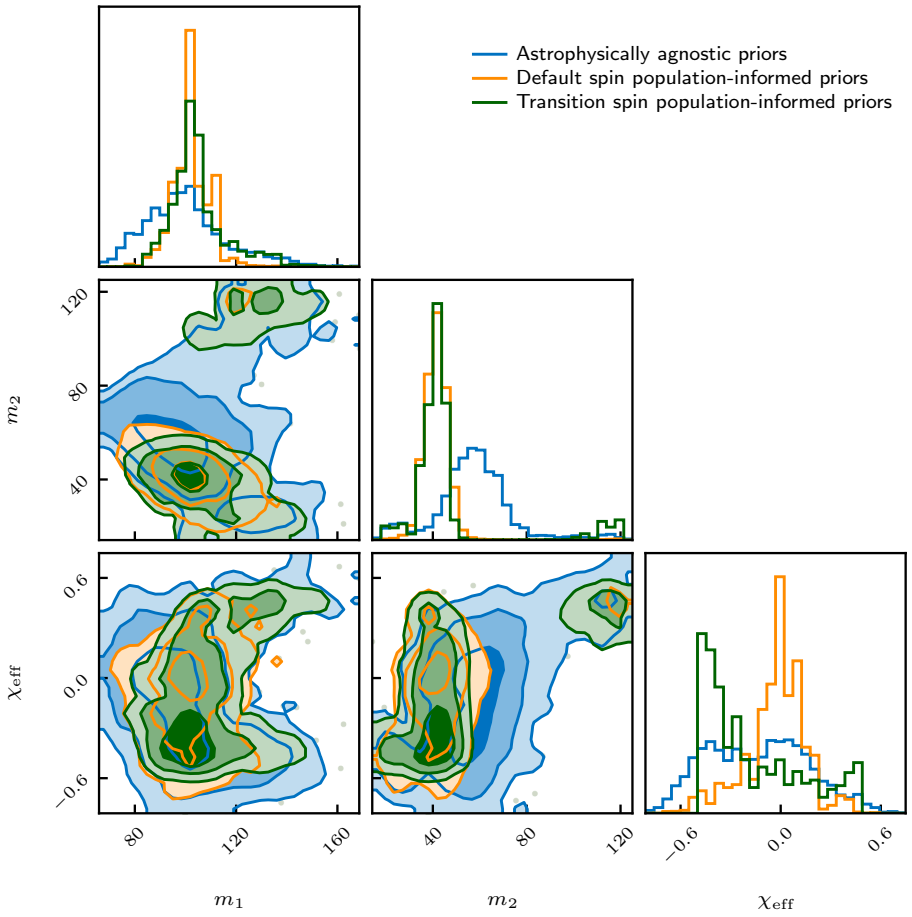

Extended Figure 10 The inferred population-informed estimates of the primary mass m_1, secondary mass m_2, and effective spin $\chi_{\rm eff}$ for GW190521. The contours represent 1, 2, 3-sigma credible regions respectively.

The analyses in this work were carried out by Tong. Fishbach and Thrane served as Tong's supervisors, providing guidance and assisting with the writing of the manuscript. Additional support was provided by Mould, Callister, Farah, and Banagiri, who provided suggestions for analyses and helped interpret the results. Guttman performed the maximum population likelihood distribution analysis. Mould contributed to the initial code development. Galaudage helped with plotting. Beltran-Martinez, Farr, Galaudage, Godrey, Heinzel, Kalomenopoulos, Miller and Vijaykumar contributed to the conception of this work. All authors contributed to editing the manuscript.

Corresponding author
Correspondence to Hui Tong.

Competing interests
The authors declare that they have no competing financial interests.

References

[1] Fowler, W.A., Hoyle, F.: Neutrino Processes and Pair Formation in Massive Stars and Supernovae. Astrophys. J. Suppl. **9**, 201–319 (1964)

[2] Rakavy, G., Shaviv, G.: Instabilities in Highly Evolved Stellar Models. Astrophys. J. **148**, 803 (1967)

[3] Barkat, Z., Rakavy, G., Sack, N.: Dynamics of supernova explosion resulting from pair formation. Phys. Rev. Lett. **18**, 379–381 (1967)

[4] Fraley, G.S.: Supernovae Explosions Induced by Pair-Production Instability. Ap&SS **2**(1), 96–114 (1968)

[5] Heger, A., Woosley, S.E.: The nucleosynthetic signature of population III. Astrophys. J. **567**, 532–543 (2002)

[6] Woosley, S.E., Blinnikov, S., Heger, A.: Pulsational pair instability as an explanation for the most luminous supernovae. Nature **450**, 390 (2007)

[7] Farmer, R., Renzo, M., de Mink, S.E., Marchant, P., Justham, S.: Mind the Gap: The Location of the Lower Edge of the Pair-instability Supernova Black Hole Mass Gap. Astrophys. J. **887**(1), 53 (2019)

[8] Schulze, S., *et al.*: 1100 days in the life of the supernova 2018ibb - The best pair-instability supernova candidate, to date. Astron. Astrophys. **683**, 223 (2024)

[9] Angus, C.R., *et al.*: Double acct: a distinct double-peaked supernova matching pulsational pair-instability models. Astrophys. J. Lett. **977**, 41 (2024)

[10] Aasi, J., *et al.*: Advanced LIGO. Class. Quant. Grav. **32**, 074001 (2015)

[11] Acernese, F., *et al.*: Advanced Virgo: a second-generation interferometric gravitational wave detector. Class. Quant. Grav. **32**, 024001 (2015)

[12] Akutsu, T., *et al.*: Overview of KAGRA: Detector design and construction history. PTEP **2021**(5), 05–101 (2021)

[13] Farmer, R., Renzo, M., Mink, S., Fishbach, M., Justham, S.: Constraints from gravitational wave detections of binary black hole mergers on the $^{12}\mathrm{C}\,(\alpha,\gamma)^{16}\mathrm{O}$ rate. Astrophys. J. Lett. **902**(2), 36 (2020)

[14] Abbott, R., *et al.*: The population of merging compact binaries inferred using gravitational waves through GWTC-3. Phys. Rev. X **13**, 011048 (2023)

[15] Edelman, B., Doctor, Z., Farr, B.: Poking Holes: Looking for Gaps in LIGO/Virgo's Black Hole Population. Astrophys. J. Lett. **913**(2), 23 (2021)

[16] Mould, M., Gerosa, D., Taylor, S.R.: Deep learning and Bayesian inference of gravitational-wave populations: Hierarchical black-hole mergers. Phys. Rev. D **106**(10), 103013 (2022)

[17] Wang, Y.-Z., Li, Y.-J., Vink, J.S., Fan, Y.-Z., Tang, S.-P., Qin, Y., Wei, D.-M.: Potential Subpopulations and Assembling Tendency of the Merging Black Holes. Astrophys. J. Lett. **941**(2), 39 (2022)

[18] Li, Y.-J., Wang, Y.-Z., Tang, S.-P., Fan, Y.-Z.: Resolving the Stellar-Collapse and Hierarchical-Merger Origins of the Coalescing Black Holes. Phys. Rev. Lett. **133**(5), 051401 (2024)

[19] Antonini, F., Romero-Shaw, I.M., Callister, T.: Star cluster population of high mass black hole mergers in gravitational wave data. Phys. Rev. Lett. **134**, 011401 (2025)

[20] Abbott, B.P., Abbott, R., Abbott, T.D., Abraham, S., Acernese, F., Ackley, K., Adams, C., Adhikari, R.X., Adya, V.B., Affeldt, C., al.: Binary Black Hole Population Properties Inferred from the First and Second Observing Runs of Advanced LIGO and Advanced Virgo. Astrophys. J. Lett. **882**(2), 24 (2019)

[21] Abbott, R., Abbott, T.D., Abraham, S., Acernese, F., al.: Population properties of compact objects from the second LIGO–virgo gravitational-wave transient catalog. The Astrophysical Journal Letters **913**, 7 (2021)

[22] Talbot, C., Thrane, E.: Measuring the binary black hole mass spectrum with an astrophysically motivated parameterization. Astrophys. J. **856**, 173 (2018)

[23] Golomb, J., Isi, M., Farr, W.M.: Physical Models for the Astrophysical Population of Black Holes: Application to the Bump in the Mass Distribution of Gravitational-wave Sources. Astrophys. J. **976**(1), 121 (2024)

[24] Stevenson, S., Sampson, M., Powell, J., Vigna-Gómez, A., Neijssel, C.J., Szécsi, D., Mandel, I.: The impact of pair-instability mass loss on the binary black hole mass distribution (2019)

[25] Croon, D., Sakstein, J.: Prediction of Multiple Features in the Black Hole Mass Function due to Pulsational Pair-Instability Supernovae (2023) arXiv:2312.13459

[26] Gerosa, D., Fishbach, M.: Hierarchical mergers of stellar-mass black holes and their gravitational-wave signatures. Nature **5** (2021)

[27] Di Carlo, U.N., Giacobbo, N., Mapelli, M., Pasquato, M., Spera, M., Wang, L., Haardt, F.: Merging black holes in young star clusters. Mon. Not. Roy. Astron. Soc. **487**(2), 2947–2960 (2019)

[28] Renzo, M., Cantiello, M., Metzger, B.D., Jiang, Y.-F.: The Stellar Merger Scenario for Black Holes in the Pair-instability Gap. Astrophys. J. Lett. **904**(2), 13 (2020)

[29] Siegel, D.M., Agarwal, A., Barnes, J., Metzger, B.D., Renzo, M., Villar, V.A.: "Super-kilonovae" from Massive Collapsars as Signatures of Black Hole Birth in the Pair-instability Mass Gap. Astrophys. J. **941**(1), 100 (2022)

[30] McKernan, B., Ford, K.E.S., Lyra, W., Perets, H.B.: Intermediate mass black holes in AGN discs - I. Production and growth. Mon. Not. R. Ast. Soc. **425**(1), 460–469 (2012)

[31] Safarzadeh, M., Haiman, Z.: Formation of GW190521 via gas accretion onto Population III stellar black hole remnants born in high-redshift minihalos. Astrophys. J. Lett. **903**(1), 21 (2020)

[32] Abac, A.G., et al.: GWTC-4.0: Updating the Gravitational-Wave Transient Catalog with Observations from the First Part of the Fourth LIGO-Virgo-KAGRA Observing Run (2025) arXiv:2508.18082 [gr-qc]

[33] Abac, A.G., et al.: GWTC-4.0: Population Properties of Merging Compact Binaries (2025) arXiv:2508.18083 [astro-ph.HE]

[34] Woosley, S.E.: Pulsational Pair-Instability Supernovae. Astrophys. J. **836**(2), 244 (2017)

[35] Abac, A.G., et al.: GW231123: a Binary Black Hole Merger with Total Mass 190-265 $M_\odot$ (2025) arXiv:2507.08219 [astro-ph.HE]

[36] Gottlieb, O., Metzger, B.D., Issa, D., Li, S.E., Renzo, M., Isi, M.: Spinning into the Gap: Direct-Horizon Collapse as the Origin of GW231123 from End-to-End GRMHD Simulations (2025) arXiv:2508.15887 [astro-ph.HE]

[37] Payne, E., Thrane, E.: Model exploration in gravitational-wave astronomy with the maximum population likelihood. Phys. Rev. Res. **5**, 023013 (2023)

[38] Abbott, R., *et al.*: GWTC-3: Compact Binary Coalescences Observed by LIGO and Virgo During the Second Part of the Third Observing Run. Phys. Rev. X **13**, 041039 (2023)

[39] Fitchett, M.J.: The influence of gravitational wave momentum losses on the centre of mass motion of a newtonian binary system. Monthly Notices of the Royal Astronomical Society **203**(4), 1049–1062 (1983)

[40] Gerosa, D., Hébert, F., Stein, L.C.: Black-hole kicks from numerical-relativity surrogate models. Phys. Rev. D **97**(10), 104049 (2018)

[41] Antonini, F., Rasio, F.A.: Merging black hole binaries in galactic nuclei: implications for advanced-LIGO detections. Astrophys. J. **831**(2), 187 (2016)

[42] Rodriguez, C.L., Zevin, M., Amaro-Seoane, P., Chatterjee, S., Kremer, K., Rasio, F.A., Ye, C.S.: Black holes: The next generation—repeated mergers in dense star clusters and their gravitational-wave properties. Phys. Rev. D **100**(4), 043027 (2019)

[43] Antonini, F., Romero-Shaw, I., Callister, T., Dosopoulou, F., Chattopadhyay, D., Gieles, M., Mapelli, M.: Gravitational waves reveal the pair-instability mass gap and constrain nuclear burning in massive stars (2025) arXiv:2509.04637 [astro-ph.HE]

[44] Damour, T.: Coalescence of two spinning black holes: An effective one-body approach. Phys. Rev. D **64**, 124013 (2001)

[45] McKernan, B., Ford, K.E.S.: Constraining the LVK AGN channel with black hole spins. Mon. Not. Roy. Astron. Soc. **531**(3), 3479–3485 (2024) https://doi.org/10.1093/mnras/stae1351

[46] Fishbach, M., Holz, D.E.: Minding the gap: Gw190521 as a straddling binary. The Astrophysical Journal Letters **904**(2), 26 (2020)

[47] deBoer, R.J., Görres, J., Wiescher, M., Azuma, R.E., Best, A., Brune, C.R., Fields, C.E., Jones, S., Pignatari, M., Sayre, D., Smith, K., Timmes, F.X., Uberseder, E.: The $^{12}\mathbf{C}(\alpha,\gamma)^{16}\mathbf{O}$ reaction and its implications for stellar helium burning. Rev. Mod. Phys. **89**, 035007 (2017)

[48] Buchmann, L.: New Stellar Reaction Rate for 12C(alpha , gamma) 16O. Astrophys. J. Lett. **468**, 127 (1996) https://doi.org/10.1086/310240

[49] Kunz, R., Fey, M., Jaeger, M., Mayer, A., Hammer, J.W., Staudt, G., Harissopulos, S., Paradellis, T.: Astrophysical Reaction Rate of ^{12}C(α, γ)^{16}O. Astrophys. J. **567**(1), 643–650 (2002) https://doi.org/10.1086/338384

[50] Shen, Y., *et al.*: New Determination of the ^{12}C(α, γ)^{16}O Reaction Rate and Its Impact on the Black-hole Mass Gap. Astrophys. J. **945**(1), 41 (2023)

[51] Farr, W.M., Fishbach, M., Ye, J., Holz, D.E.: A future percent-level measurement of the hubble expansion at redshift 0.8 with advanced ligo. The Astrophysical Journal Letters **883**, 42 (2019)

[52] Talbot, C., Farah, A., Galaudage, S., Golomb, J., Tong, H.: GWPopulation: Hardware agnostic population inference for compact binaries and beyond. J. Open

Source Softw. **10**(109), 7753 (2025)

[53] Fishbach, M., Holz, D.E., Farr, W.M.: Does the Black Hole Merger Rate Evolve with Redshift? Astrophys. J. Lett. **863**(2), 41 (2018)

[54] Thrane, E., Talbot, C.: An introduction to bayesian inference in gravitational-wave astronomy: Parameter estimation, model selection, and hierarchical models. Publications of the Astronomical Society of Australia **36** (2019)

[55] Mandel, I., Farr, W.M., Gair, J.R.: Extracting distribution parameters from multiple uncertain observations with selection biases. Monthly Notices of the Royal Astronomical Society **486**(1), 1086–1093 (2019)

[56] Vitale, S., Gerosa, D., Farr, W.M., Taylor, S.R.: Inferring the properties of a population of compact binaries in presence of selection effects (2020) arXiv:2007.05579 [astro-ph.IM]

[57] Abac, A.G., et al.: GWTC-4.0: Methods for Identifying and Characterizing Gravitational-wave Transients (2025) arXiv:2508.18081 [gr-qc]

[58] Buikema, A., *et al.*: Sensitivity and performance of the Advanced LIGO detectors in the third observing run. Phys. Rev. D **102**(6), 062003 (2020)

[59] Ganapathy, D., *et al.*: Broadband Quantum Enhancement of the LIGO Detectors with Frequency-Dependent Squeezing. Physical Review X **13**(4), 041021 (2023)

[60] Jia, W., *et al.*: Squeezing the quantum noise of a gravitational-wave detector below the standard quantum limit. Science **385**(6715), 1318 (2024)

[61] Capote, E., *et al.*: Advanced LIGO detector performance in the fourth observing run. Phys. Rev. D **111**(6), 062002 (2025)

[62] Soni, S., *et al.*: LIGO Detector Characterization in the first half of the fourth Observing run. Class. Quant. Grav. **42**(8), 085016 (2025)

[63] Tiwari, V.: Estimation of the Sensitive Volume for Gravitational-wave Source Populations Using Weighted Monte Carlo Integration. Class. Quant. Grav. **35**(14), 145009 (2018)

[64] Farr, W.M.: Accuracy Requirements for Empirically Measured Selection Functions. Research Notes of the American Astronomical Society **3**(5), 66 (2019)

[65] Essick, R., Farr, W.: Precision Requirements for Monte Carlo Sums within Hierarchical Bayesian Inference (2022) [astro-ph.IM]. arxiv/2204.00461

[66] Essick, R., et al.: Compact Binary Coalescence Sensitivity Estimates with Injection Campaigns during the LIGO-Virgo-KAGRA Collaborations' Fourth Observing Run (2025) arXiv:2508.10638 [gr-qc]

[67] Ashton, G., Hübner, M., Lasky, P.D., *et al.*: Bilby: A user-friendly bayesian inference library for gravitational-wave astronomy. The Astrophysical Journal Supplement Series **241**(2), 27 (2019)

[68] Romero-Shaw, I.M., Talbot, C., *et al.*: Bayesian inference for compact binary coalescences with bilby: validation and application to the first ligo–virgo gravitational-wave transient catalogue. Monthly Notices of the Royal Astronomical Society **499**(3), 3295–3319 (2020)

[69] Speagle, J.S.: DYNESTY: a dynamic nested sampling package for estimating Bayesian posteriors and evidences. Mon. Not. R. Ast. Soc. **493**(3), 3132–3158 (2020)

[70] Abbott, R., *et al.*: GWTC-2.1: Deep extended catalog of compact binary coalescences observed by LIGO and Virgo during the first half of the third observing run. Phys. Rev. D **109**(2), 022001 (2024)

[71] Abbott, R., *et al.*: Properties and Astrophysical Implications of the $150M_{\odot}$ Binary Black Hole Merger GW190521. Astrophys. J. Lett. **900**, 13 (2020)

[72] Woosley, S.E.: The evolution of massive helium stars, including mass loss. The Astrophysical Journal **878**(1), 49 (2019)

[73] Fishbach, M., Essick, R., Holz, D.E.: Does Matter Matter? Using the mass distribution to distinguish neutron stars and black holes. Astrophys. J. Lett. **899**, 8 (2020)

[74] Farah, A.M., Fishbach, M., Holz, D.E.: Two of a Kind: Comparing Big and Small Black Holes in Binaries with Gravitational Waves. Astrophys. J. **962**(1), 69 (2024)

[75] Antonini, F., Callister, T., Dosopoulou, F., Romero-Shaw, I., Chattopadhyay, D.: Inferring the pair-instability mass gap from gravitational wave data using flexible models (2025) arXiv:2506.09154 [astro-ph.HE]

[76] Abbott, R., *et al.*: GW190521: A Binary Black Hole Merger with a Total Mass of $150M_{\odot}$. Phys. Rev. Lett. **125**, 101102 (2020)

[77] Doctor, Z., Wysocki, D., O'Shaughnessy, R., Holz, D.E., Farr, B.: Black hole coagulation: Modeling hierarchical mergers in black hole populations. The Astrophysical Journal **893**(1), 35 (2020)

[78] Kimball, C., Talbot, C., Berry, C.P.L., Carney, M., Zevin, M., Thrane, E., Kalogera, V.: Black hole genealogy: Identifying hierarchical mergers with gravitational waves. Astrophys. J. **900**, 177 (2020)

[79] Kimball, C., *et al.*: Evidence for Hierarchical Black Hole Mergers in the Second

LIGO–Virgo Gravitational Wave Catalog. Astrophys. J. Lett. **915**(2), 35 (2021)

[80] Tong, H., et al.: Evidence of the Pair Instability Gap in the Distribution of Black Hole Masses Data Release. https://doi.org/10.5281/zenodo.18222409

[81] Collaboration, L.S., Collaboration, V., Collaboration, K.: GWTC-4.0: Parameter Estimation Data Release. https://doi.org/10.5281/zenodo.16053484

[82] Collaboration, L.S., Collaboration, V.: GWTC-2.1: Deep Extended Catalog of Compact Binary Coalescences Observed by LIGO and Virgo During the First Half of the Third Observing Run - Parameter Estimation Data Release. https://doi.org/10.5281/zenodo.6513631

[83] Collaboration, L.S., Collaboration, V., Collaboration, K.: GWTC-3: Compact Binary Coalescences Observed by LIGO and Virgo During the Second Part of the Third Observing Run — Parameter Estimation Data Release. https://doi.org/10.5281/zenodo.5546663

[84] Collaboration, L.S., Collaboration, V., Collaboration, K.: GWTC-4.0 Cumulative Search Sensitivity Estimates. https://doi.org/10.5281/zenodo.16740128